

Structural phase transition and transport properties in topological material candidate $NaZn_4As_3$

Qing-Xin Dong(董庆新), Bin-Bin Ruan(阮彬彬), Yi-Fei Huang(黄奕飞), Yi-Yan Wang(王义炎), Li-Bo Zhang(张黎博), Jian-Li Bai(白建利), Qiao-Yu Liu(刘乔宇), Jing-Wen Cheng(程靖雯), Zhi-An Ren(任治安), and Gen-Fu Chen(陈根富)

Citation: Chin. Phys. B, 2023, 32 (**6**): 066501. DOI: 10.1088/1674-1056/acbe2f
Journal homepage: http://cpb.iphy.ac.cn; http://iopscience.iop.org/cpb

What follows is a list of articles you may be interested in

Lattice thermal conductivity switching via structural phase transition in ferromagnetic VI_3

Chao Wu(吴超) and Chenhan Liu(刘晨晗)
Chin. Phys. B, 2023, 32 (**5**): 056502. DOI: 10.1088/1674-1056/acb764

Near-zero thermal expansion in β-$CuZnV_2O_7$ in a large temperature range

Yaguang Hao(郝亚光), Hengli Xie(谢恒立), Gaojie Zeng(曾高杰), Huanli Yuan(袁焕丽), Yangming Hu(胡杨明), Juan Guo(郭娟), Qilong Gao(高其龙), Mingju Chao(晁明举), Xiao Ren(任霄), and Er-Jun Liang(梁二军)
Chin. Phys. B, 2022, 31 (**4**): 046502. DOI: 10.1088/1674-1056/ac3393

Tuning thermal transport via phonon localization in nanostructures

Dengke Ma(马登科), Xiuling Li(李秀玲), and Lifa Zhang(张力发)
Chin. Phys. B, 2020, 29 (**12**): 126502. DOI: 10.1088/1674-1056/abb7fa

Low lattice thermal conductivity and high figure of merit in p-type doped K_3IO

Weiqiang Wang(王巍强), Zhenhong Dai(戴振宏), Qi Zhong(钟琦), Yinchang Zhao(赵银昌), and Sheng Meng(孟胜)
Chin. Phys. B, 2020, 29 (**12**): 126501. DOI: 10.1088/1674-1056/abab83

Thermal transport in phosphorene and phosphorene-based materials: A review on numerical studies

Yang Hong(洪扬), Jingchao Zhang(张景超), Xiao Cheng Zeng(曾晓成)
Chin. Phys. B, 2018, 27 (**3**): 036501. DOI: 10.1088/1674-1056/27/3/036501

Structural phase transition and transport properties in topological material candidate $NaZn_4As_3$

Qing-Xin Dong(董庆新)[1,2], Bin-Bin Ruan(阮彬彬)[1], Yi-Fei Huang(黄奕飞)[1,2], Yi-Yan Wang(王义炎)[4], Li-Bo Zhang(张黎博)[1,2], Jian-Li Bai(白建利)[1,2], Qiao-Yu Liu(刘乔宇)[1,2], Jing-Wen Cheng(程靖雯)[1,2], Zhi-An Ren(任治安)[1,2,3], and Gen-Fu Chen(陈根富)[1,2,3,†]

[1] *Institute of Physics and Beijing National Laboratory for Condensed Matter Physics, Chinese Academy of Sciences, Beijing* 100190, *China*
[2] *School of Physical Sciences, University of Chinese Academy of Sciences, Beijing* 100049, *China*
[3] *Songshan Lake Materials Laboratory, Dongguan* 523808, *China*
[4] *Institute of Physical Science and Information Technology, Anhui University, Hefei* 230601, *China*

(Received 2 February 2023; revised manuscript received 2 February 2023; accepted manuscript online 23 February 2023)

We report a comprehensive study on a layered-structure compound of $NaZn_4As_3$, which has been predicted to be an ideal topological semimetal (TSM) candidate. It is found that $NaZn_4As_3$ undergoes a structural transformation from high temperature rhombohedral to a low temperature monoclinic phase. The electric resistivity exhibits a metal-to-insulator-like transition at around 100 K, and then develops a plateau at low temperature, which might be related to the protected topologically conducting surface states. Our first-principles calculation confirms further that $NaZn_4As_3$ is a topological insulator (TI) for both different phases rather than a previously proposed TSM. The Hall resistivity reveals that the hole carriers dominate the transport properties for the whole temperature range investigated. Furthermore, an obvious kink possibly associated to the structure transition has been detected in thermopower around $\sim$ 170 K. The large thermopower and moderate κ indicate that $NaZn_4As_3$ and /or its derivatives can provide a good platform for optimizing and studying the thermoelectric performance.

Keywords: structural phase transition, thermoelectric, topological materials, crystal growth

PACS: 65.40.–b, 71.30.+h, 75.47.–m, 81.10.–h **DOI:** 10.1088/1674-1056/acbe2f

1. Introduction

Transition-metal pnictides and chalcogenides have captivated intense researchers' interests and attentions in condensed matter physics and material science due to the discovery of high temperature superconductivity,[1,2] high thermoelectric performance,[3–5] and other unique and exceptional properties.[6,7] These compounds are significant in their own right because of their distinct chemically structure.[8–15] Recently, a series of compounds with a new Zintl phases, composed of the alkali metal A, d^{10} transition metal T, and pnictide Pn (A = Na, K, Rb or Cs, T = Cd, Zn, and Pn = P, As) in the general formula AT_4Pn_3, have been reported.[10] All of them can be divided into two categories depending on the structure: one subgroup crystallizes in the KCu_4S_3-type structure (space group P_4/mmm, $Z = 1$, Pearson symbol $tP8$) and the other adopts $RbCd_4As_3$ structure type (R-3m, $Z = 3$, Pearson symbol $hR24$). Both of them can be regarded as the result of inserting a layer of alkali metal ions into the main framework composed of $[T_4Pn_3]^{-1}$ layer. It also provides a research idea for the synthesis of new compounds with novel and multi-layered structures. Although most combinations have been realized, many of these materials have not been systematically studied, apart from structural information. In addition, with the proposal and development of topology, some of them are even predicted to be topological materials with topologically protected nontrivial band structure.[16–18] Take $NaCd_4As_3$ as an example,[19] it undergoes a topological phase transition from topological crystalline insulator to topological insulator (TI) induced by the structural phase transition, which provides rich topological information and attracts more researchers to pay more attention to their topological properties.

Motivated by the consideration above, in this work, we focus on the $NaZn_4As_3$, which has been predicted to be a candidate of ideal Dirac semimetal.[17,18,20] The systematic study on magneto-transport and thermoelectric properties of $NaZn_4As_3$ have been performed. Crystallographic investigation shows that it undergoes a structural transformation from the rhombohedral structure in space group R-3m to a monoclinic phase with decreasing temperature. A metal-to-insulator-like transition and a low-temperature resistivity plateau have been observed. The latter has been taken as a transport signature of conducting surface states protected by time reversal symmetry. The Hall resistivity shows positive quasi-linear behavior and reveals the typical hole density is in the order of $\sim 10^{18}$ cm^{-3}. All of those indicates the $NaZn_4As_3$ is more likely to be a TI, and confirms further by our first-principles calculations. An obvious kink is detected in the thermopower around $\sim$ 170 K, at which the structure transi-

†Corresponding author. E-mail: gfchen@iphy.ac.cn

© 2023 Chinese Physical Society and IOP Publishing Ltd

tion may happen. However, no anomaly appears in the specific heat at such temperature. The thermoelectric properties reveal a large thermopower of ~ 360 μV/K and a moderate κ of ~ 6 W·m^{-1}·K^{-1} at room temperature. All of these make $NaZn_4As_3$ to be a good platform for investigating the relationship between the topological state and thermoelectrics.

2. Experiment and method

High-quality single crystals of $NaZn_4As_3$ were grown from zinc flux. The starting elements Na, Zn, and As were mixed with an optimized molar ratio of Na:Zn:As = 1:8:3 and put into an alumina crucible covered with quartz wool. The crucible was sealed in a quartz tube and heated to 1123 K, kept at this temperature for 10 h, and then cooled down to 823 K over 200 hours, at which the Zn flux was separated from the crystals using a centrifuge. The obtained $NaZn_4As_3$ single crystals are in the form of sheet shape with typical size of 2 mm × 1 mm × 0.2 mm, as shown in the inset of Fig. 1(d). Powder and surface planes diffraction (XRD) patterns were collected by PANalytical x-ray diffractometer with Cu $K\alpha$ radiation ($\lambda = 1.541874$ Å) and PC-GSAS.[21] was employed for the data refinement. The determinations of the single crystals were carried out on a single crystal diffractometer of BRUKER D8 VENTURE and refined using the Bruker SHELXTL software package. The atomic proportions of the obtained crystals were checked by Oxford x-Max energy dispersive x-ray (EDX) spectroscopy analysis in a Hitachi S-4800 scanning electron microscope. Electric and thermal transport properties measurements were performed in a physical property measurement system (Quantum Design PPMS-9 T) with a temperature range from 2 K to 300 K. First-principles calculations were carried out using the Quantum ESPRESSO package.[22] Projector augmented wave pseudopotentials based on the exchange–correlation functionals of PBEsol were used.[23,24] Experimental crystallographic parameters were adopted without relaxation. We applied a Monkhorst–Pack grid of 15 × 15 × 15 in the self-consistent calculations. The energy cutoffs for wavefuntions and charge densities were 70 Ry (1 Ry = 13.6056923 eV) and 500 Ry, respectively.

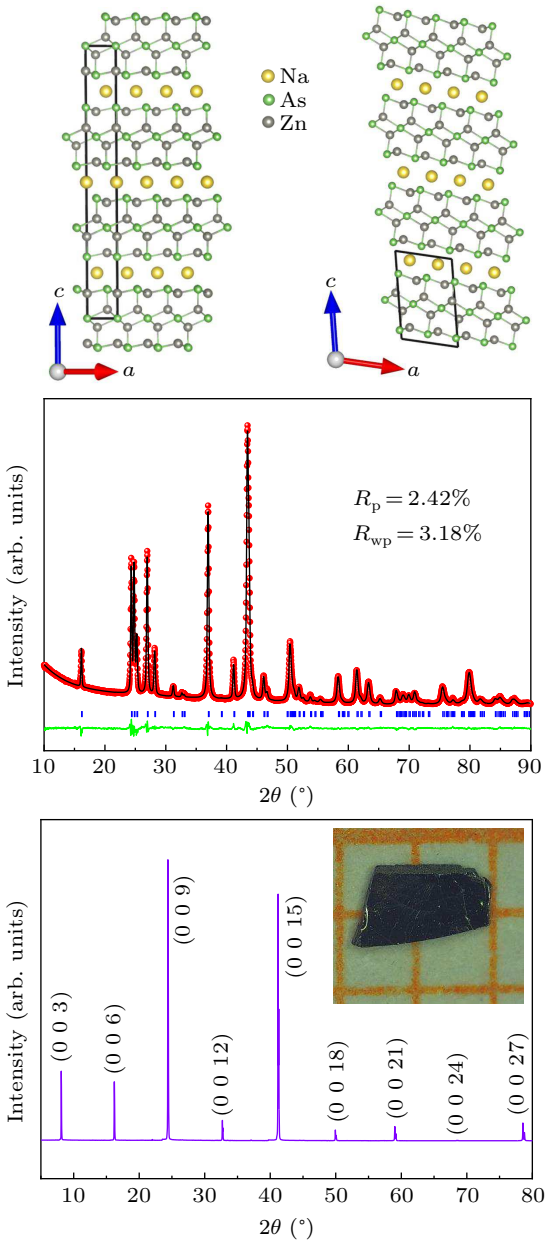


Fig. 1. The crystal structures of $NaZn_4As_3$ projected along *b* axis at (a) 298 K and (b) 100 K, respectively. The black lines, the yellow, gray, and light green balls represent the unit cell, Na, Zn, As atoms, respectively. (c) Rietveld analysis of the powder XRD pattern of $NaZn_4As_3$. Red balls and black solid line represent the experiment data and calculated curve, respectively. The difference curve is plotted in the green line. The vertical blue lines denote the positions of Bragg peaks. (d) Single crystal XRD pattern collected at room temperature. Inset: A typical optical image of the grown crystal on millimeter paper.

3. Results and discussion

Different from the KCu_4S_3-type structure homologous compounds of KZn_4As_3 and $RbZn_4As_3$,[10] $NaZn_4As_3$ is isostructural with $NaCd_4As_3$, which crystallizes in rhombohedral structure with space group *R*-3*m* (No. 166), and is composed of alternating $[Zn_4As_3]^-$ layers and Na^+ cations layers, as shown in Fig. 1(a). More specifically, the Zn, As1, and As2 atoms occupy the 6*c*, 6*c*, and 3*a* Wyckoff sites, respectively, and form the $[Zn_4As_3]^-$ main layers; while Na atoms, located at 3*b* Wyckoff site, fill in the interspace as the interstitial atoms and form Na^+ cations layers. When temperature falls down to 100 K, the structure remains the layered configuration but has a slight distortion in the *ab* plane, leading to the breaking of the mirror symmetry and forming a monoclinic phase with *C*1*m*1 (No. 8) space group, as shown in Fig. 1(b), which is similar to that of the $NaCd_4As_3$.[19] In this structure, As1 and As2 atoms are located in 2*a* Wyckoff sites, causing a dramatic change of *c* from 32.83 Å to 11.15 Å. Meanwhile, the unit lattice of *a* increases into 7.18 Å from 4.16 Å but *b* remains nearly un-

changed. More detailed refinement results are listed in the Table 1. Figure 1(c) shows the powder XRD pattern and Rietveld refinement result of $NaZn_4As_3$ at room temperature. All the reflections can be well indexed in the *R*-3*m* (No. 166) space group with small reliability factors $R_p = 2.42\%$, $R_{wp} = 3.18\%$, indicating the high quality of single crystals. The determined lattice parameters are $a = b = 4.16$ Å and $c = 32.83$ Å, which are consistent with those of the single crystal refinement. The single crystal XRD pattern presented in Fig. 1(d) indicates that the plane of the crystal is (0 0 3*l*) crystallographic plane.

Table 1. Crystal data and structure refinement for $NaZn_4As_3$.

Empirical formula	$NaZn_4As_3$	$NaZn_4As_3$
T (K)	298	100
Crystal system	trigonal	monoclinic
Space group	*R*-3*m*	*C*1*m*1
a (Å)/α	4.1640(8)/90°	7.1791(16)/90°
b (Å)/β	4.1640(8)/90°	4.1481(10)/102.326°
c (Å)/γ	32.848(9)/120°	11.151(3)/90°
V (Å^3)	493.2(2)	324.42(14)
Molar mass (g/mol)	509.23	509.23
Density (g/cm^3)	5.143	5.213
θ range (°)	3.72 ~ 28.29	3.74 ~ 25.59
Radiation type	Mo Kα	Mo Kα
Wavelength (Å)	0.71073	0.71073
Z	3	2
Absorption coefficient	multi-scan	multi-scan
Structure solution technique	direct methods	direct methods
Refinement method	full-matrix least-squares on F^2	full-matrix least-squares on F^2
Reflections collected	1230	2023
Independent reflections	194 [$R_{int} = 0.0623$]	844 [$R_{int} = 0.0495$]
Largest diff. peak and hole	3.702 and −1.366 e·Å^{-3}	2.512 and −3.146 e·Å^{-3}
Final R^a indices [$I > 2\sigma(I)$]	$R1 = 0.0527$, $wR2 = 0.1415$	$R1 = 0.0450$, $wR2 = 0.1205$
R indices (all data)	$R1 = 0.0547$, $wR2 = 0.1432$	$R1 = 0.0461$, $wR2 = 0.1221$
Goodness-of-fit on F^2	1.261	1.113

The electric transport properties measured on $NaZn_4As_3$ single crystal S1 (1.2 mm × 0.3 mm × 0.07 mm) with or without applied magnetic field $\mu_0 H$ are summarized in Fig. 2. Clearly, the evolution of resistivity with temperature (Fig. 2(a)) is not monotonous. At zero field, the temperature-dependent $\rho_{xx}(T)$ first decreases rapidly with decreasing temperature, exhibiting a metallic behavior until ~ 100 K. Thereafter the $\rho_{xx}(T)$ starts to increase slightly and tends to saturate, developing a resistivity plateau at low temperature. The resistivity plateau, which has been observed more frequently in TIs, such as SmB_6,[25] Bi_2Te_2Se,[26] Bi_2Te_3,[27] and $TlBi_xSb_{1-x}Te_2$,[28] and has been taken as a transport signature of conducting surface states of TIs protected by time reversal symmetry. An applied magnetic field $\mu_0 H = 9$ T does hardly change the resistivity behavior in high temperature regime, except for the downward translation of the resistivity platform in the low temperature zone, leading to the emergence of negative magneto-resistance (MR).

To investigate the origin of negative MR, the magnetic field dependence of MR at various temperatures with applied field $\mu_0 H$ parallel and perpendicular to current I are shown in Figs. 2(b) and 2(c), respectively. As the temperature T increases, the negative longitudinal MR ($\mu_0 H \parallel I$) gradually suppressed. Such phenomenon is indeed observed in many TSMs,[29–32] in which the negative MR is caused by the charge pumping when the applied magnetic field is parallel to the current. Paradoxically, we also observed the negative MR when magnetic field is perpendicular to current, as shown in Fig. 2(c), which questions the possibility of chiral anomaly in $NaZn_4As_3$. Similarly, the increase of temperature weakens the negative MR effect in the low temperature region. When the temperature reaches above 200 K, the negative MR disappears and a minute trace of conventional positive MR (~ 0.1%) appears.

In general, the origins of negative MR can be considered to be related to following mechanisms, including spin flip[33] or magnetic scattering,[34,35] current jetting effect,[36] chiral anomaly,[29] and WL effect.[37,38] Firstly, considering that $NaZn_4As_3$ is a non-magnetic material and no magnetic impurities are found in $NaZn_4As_3$, which is corroborated by the magnetic susceptibility data (inset of Fig. 2(a)). Hence, spin flip and magnetic scattering may not be suitable reasons for the appearance of negative MR in $NaZn_4As_3$. Secondly, the negative MR resulted from the current jetting effect is commonly temperature-insensitive and highly sensitive to the contact configuration. However, the similar negative MR is also observed on the single crystal with different contact configurations. Thus, the scenario of current jetting effect does not

apply in $NaZn_4As_3$. Thirdly, chiral-anomaly-induced negative is extremely sensitive to the angle between applied filed and current, while the negative MR in $NaZn_4As_3$ appears both for $\mu_0 H \| I$ and $\mu_0 H \perp I$ configurations. Therefore, the observed negative MR in $NaZn_4As_3$ is most likely attributed to the WL effect.

In order to further understand the negative MR in $NaZn_4As_3$, the change of longitudinal conductivity

$$\sigma_{xx} = \rho_{xx}/(\rho_{xx}^2 + \rho_{xy}^2) \tag{1}$$

has been displayed in the Fig. 2(d) at selected temperatures. In the quasi-two-dimensional regime, the correction to the sheet magnetoconductance MC ($\Delta\sigma/\sigma$) produced with the magnetic field $\mu_0 H$ perpendicular to the plane is given by the following expression:[39]

$$MC = \eta(T)\left[\frac{3}{2}\Psi\left(\frac{1}{2}+\frac{B_2}{\mu_0 H}\right) - \Psi\left(\frac{1}{2}+\frac{B_1}{\mu_0 H}\right) - \frac{1}{2}\Psi\left(\frac{1}{2}+\frac{B_3}{\mu_0 H}\right) - \ln\frac{B_2^{3/2}}{B_1 B_3^{1/2}}\right], \tag{2}$$

where, $\eta(T)$, B_1, B_2, B_3 are four unknown parameters related to the elastic scattering, inelastic scattering, magnetic impurity scattering, and spin–orbit coupling; Ψ and $\mu_0 H$ are the digamma function and applied field, respectively. The inset of Fig. 2(d) shows the experimental data (black solid line) and the fitting curve (green dashed line) using aforementioned formula at 2.5 K. The high agreement of fitting curve and experiment data indicates that what causes the appearance of negative MR is the WL effect. The fitting parameters $\eta(T)$, B_1, B_2, and B_3 are 0.055 T, 0.078 T, 0.078 T, and 2.871 T, respectively. The $\eta(T)$, B_1 and B_2 are all smaller than the results from the carbon, indicating that weak elastic, inelastic and magnetic impurity scattering occur. The large parameter of B_3 reveals the strong spin–orbit scattering, which is further confirmed by our calculation. In TIs,[38,40,41] when the Fermi level is shifted from the bulk gap to the valence or conduction bands, there is a competition between the bulk electrons and surface electrons. In this case, it is possible to observe the WL effect, such as Bi_2Se_3-based materials. Furthermore, disorder[42] or defect.[36] also can induce the appearance of negative MR in TIs. This forces us to reconsider its topological classification, a TSM or a TI?

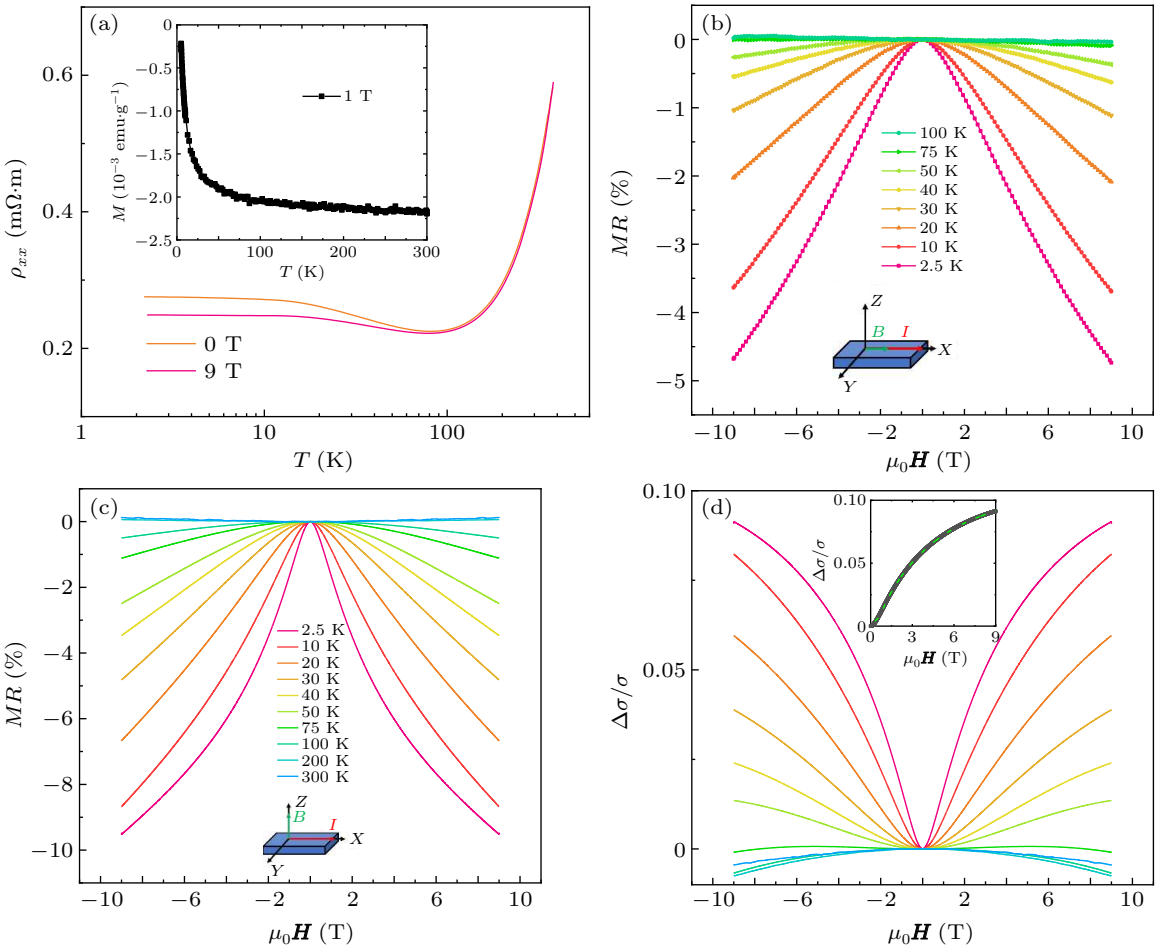


Fig. 2. The magneto-transport properties of $NaZn_4As_3$. (a) Temperature dependence of resistivity (magnetic susceptibility at 1 T for the inset) for magnetic field $\mu_0 H$ perpendicular to the current at $\mu_0 H = 0$ T and 9 T. Panels (b) and (c) are the MR at various temperatures with magnetic field $\mu_0 H$ parallel and perpendicular to the current. (d) Magnetic field dependence of magnetoconductance at selected temperatures with magnetic field perpendicular to the current. Insert: The fitting curve of MC at $T = 2.5$ K.

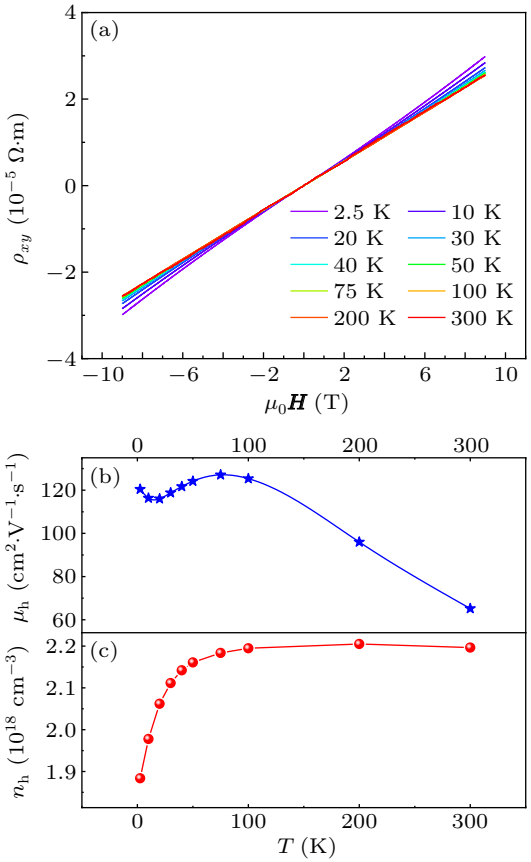


Fig. 3. (a) The field-dependent Hall resistivities at selected temperatures. Inset: The fitting of the ρ_{xy} ($\mu_0 H$) curve at 2.5 K. Panels (b) and (c) are the mobility and concentration of hole-type carrier in measured temperature range, respectively.

The carrier concentration is a helpful indicator to evaluate TSMs and TIs. In a TI, only the topologically protected surface states can conduct electrons, while the bulk state is insulating, leading to a low conduction electron concentration. However, in TSMs, the metallic bulk state allows it to have a considerable large carrier concentration. Inspired by this, we performed the measurements of field dependent Hall resistivities at various temperatures to investigate the carrier's contribution to transport process in this system. As shown in Fig. 3(a), the linear Hall resistivities and positive Hall coefficient $R_{xy} = \rho_{xy}(\mu_0 H)/\mu_0 H$ indicate that single type of hole carrier dominates the transport process. The temperature-dependent hole carrier concentration and mobility extracted from the Hall resistivities by the formula $R_{xy} = \rho_{xy}(\mu_0 H)/\mu_0 H = 1/ne$ and $\mu_H = R_{xy}/\rho_{xx}(0)$ are displayed in Figs. 3(b) and 4(c). At 2.5 K, $NaZn_4As_3$ has a hole concentration of 1.88×10^{18} cm^{-3}, and hole mobility of 120 cm^2/V·s. With the increasement of temperature, the hole concentration experiences an enhancement firstly owing to the metal-to-semiconductor like transition and remains basically unchanged above 100 K. While the carrier mobility experiences a process of first increasing and then decreasing with the increasing temperature, showing a maximum (about 130 cm^2/V·s) around 100 K. Remarkably, the concentration of hole is in the order of 10^{18} cm^{-3}, which is comparable to that of $NaCd_4As_3$[19] and have the same magnitude order as typical TI materials, such as Bi_2Se_3.[43] It is two or even more orders of magnitude lower than the carrier density of typical TSMs (10^{20} cm^{-3}–10^{21} cm^{-3}) such as WC,[44] WTe_2,[45] gray As,[46] and so on, implying $NaZn_4As_3$ is more likely to be a TI.

To better identify its topology, the electronic structures of $NaZn_4As_3$ with mentioned structures above are calculated via first-principles calculations. Figures 4(a) and 4(b) show the calculated band structures of the rhombohedral structure with ignoring and including the spin–orbital coupling (SOC) effect, respectively. Obviously, when the SOC effect is taken into account, the band inversion happens, opening the gap at Γ point. In addition, a band inversion has also been detected along the high symmetry direction from Γ to T. All of these make $NaZn_4As_3$ to be classified as a TI. We also calculated the band structure of the monoclinic phase, as shown in Figs. 4(c) and 4(d), which is similar with that of room temperature phase. When the SOC is ignored, the band inversion is absent along A to Γ and no gap emerges at Γ, suggesting the trivial band characteristic. However, with the consideration of SOC, the band inversion appears at Γ point and along A to Γ, forming a gap, which brings about the topologically protected surface states and explains why the transport properties are more like a TI rather than a TSM.

Thermodynamic measurements, specific heat and thermopower were performed to further characterize the structural phase transition. Because it reflects the average entropy of per carrier and could be affected strongly by entropy change, resulting in a better sensitivity than current to probe the energy relative to the Fermi surface density of states. The specific heat of $NaZn_4As_3$ is shown in Fig. 5(a). Regrettably, no distinct anomaly related to structural phase transition is observed in temperature-dependent specific heat measurement. Since the structural phase transition in $NaZn_4As_3$ can be seen as a slight distortion in the *ab* plane, the entropy change in this process may be very small, leading to the detection of the jump in specific heat is difficult. Figure 5(b) shows the temperature dependence of thermopower of $NaZn_4As_3$ on another sample S2 (3.5 mm × 1.5 mm × 0.2 mm). An anomalous kink can be detected around ∼ 170 K (red arrow) and the applied magnetic field hardly affect the kink, excluding the influence of magnetic impurities, which could be a sign of the structural phase transition, indicating also that thermopower measurement is a simple probe of the structural transition in $NaZn_4As_3$. The thermopower shows positive values in the whole temperature range, indicating the holes as the dominant charge carriers, which is consistent with the result from Hall resistivity measurement. The values increase as the temperature increases, reaching a promising value of 360 μV/K at

300 K, which is much larger than that of $NaCd_4As_3$,[10] but smaller than $RbZn_4As_3$.[10] As displayed in Fig. 5(c), the thermal conductivity exhibits a moderate value of $\sim 6\ W{\cdot}m^{-1}{\cdot}K^{-1}$ at room temperature and a maximum hump at low temperature due to the transition from the $\kappa_L \sim T^3$ dependence at low temperature to $\kappa_L \sim T^{-1}$ dependence at high temperature. The divergent improvement above 250 K can be attributed to the enhancement of thermal radiation at medium temperature. Notably, the carrier concentration n of $NaZn_4As_3$ is $\sim 2.0 \times 10^{18}\ cm^{-3}$ at the room temperature (Fig. 3(c)). This n value is roughly five times lower than the optimal carrier concentration $\sim 10^{19}\ cm^{-3}$ of the state-of-the-art thermoelectric materials, *e.g.*, Bi_2Te_3[47] and Mg_3Bi_2,[48] indicative of a large room to modify thermal conductivity via chemical doping, nanostructure or defect to optimize further thermoelectric performance.

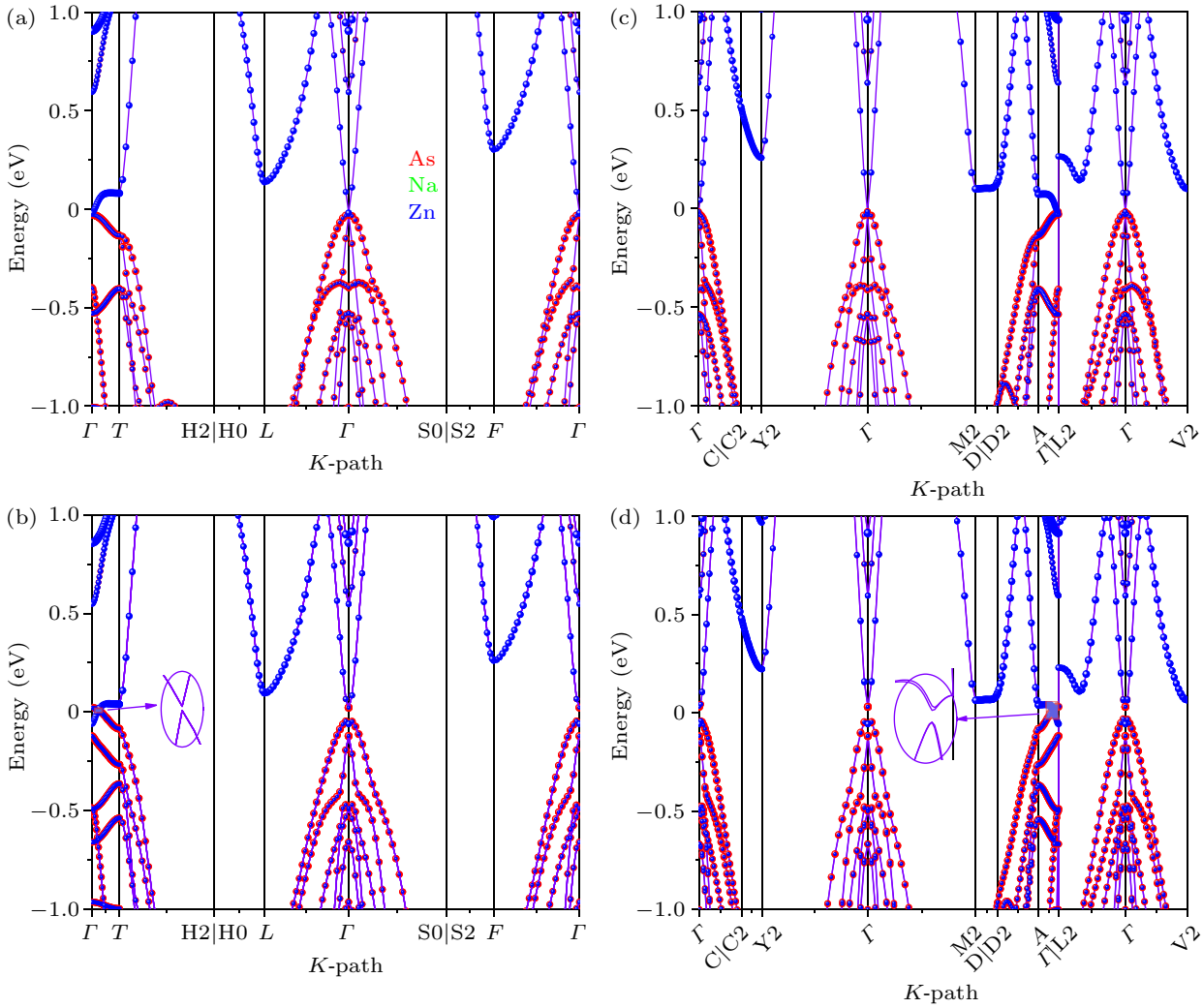


Fig. 4. Band structures of $NaZn_4As_3$. The purple line, red balls, blue balls, and green balls are representative of band structure and the contributions from As, Zn, and Na, respectively. Panels (a)/(b) and (c)/(d) are the band structures without/with SOC for the room temperature crystal structure (*R*-3*m*, No. 166) and low-temperature phase (*C*1*m*1, No. 8), respectively.

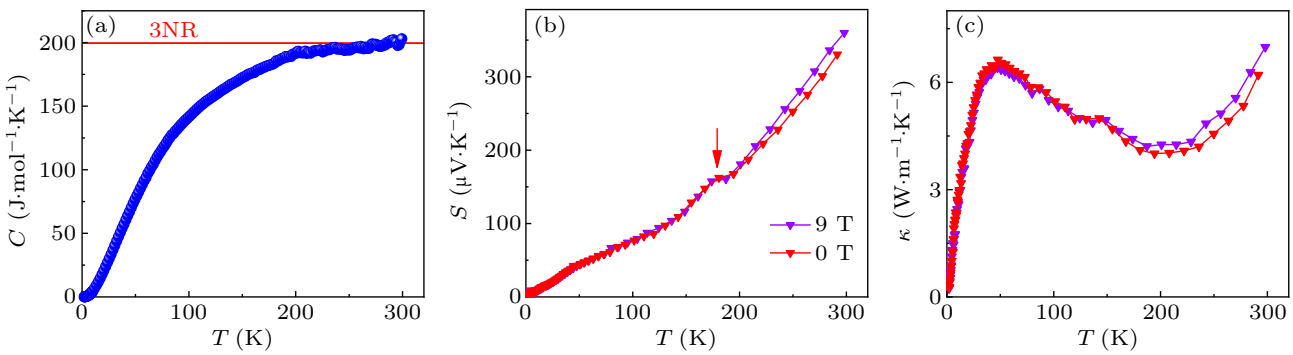


Fig. 5. (a) The temperature-dependent specific heat of $NaZn_4As_3$ from 2 K to 300 K. (b) and (c) The temperature dependence of thermopower and thermal conductivity for $NaZn_4As_3$ single crystal. An obvious kink can be detected as pointed by arrow.

4. Conclusion

In summary, single crystals of $NaZn_4As_3$ are grown and the magneto-transport, electronic structure and thermal transport properties have been studied systematically. $NaZn_4As_3$ undergoes a structural transformation from the rhombohedral structure in space group *R*-3*m* to a monoclinic phase. The measurements on thermopower suggests that the structural transition may happen around $\sim$ 170 K. The metal-to-insulator-like transition and resistivity plateau at low temperature have been observed. The WL effect leads to the emergence of negative MR. The analysis of Hall effect shows that holes are dominant carriers in transport. Combined with the electronic band structure calculations, our results indicate that $NaZn_4As_3$ is a TI rather than a TSM. Furthermore, the observed large thermopower and moderated thermal conductivity should encourage the further exploration of such materials for thermoelectric performance study.

Acknowledgments

Project supported by the National Natural Science Foundation of China (Grant Nos. 11874417 and 12274440), the Strategic Priority Research Program (B) of Chinese Academy of Sciences (Grant No. XDB33010100), and the Fund from the Ministry of Science and Technology of China (Grant No. 2022YFA1403903).

References

[1] Kamihara Y, Watanabe T, Hirano M and Hosono H 2008 *J. Am. Chem. Soc.* **130** 3296
[2] Rotter M, Tegel M and Johrendt D 2008 *Phys. Rev. Lett.* **101** 107006
[3] Zhang H, *et al.* 2008 *J. Chem. Phys.* **129** 164713
[4] Sales B, Mandrus D and Williams R K 1996 *Science* **272** 1325
[5] Gascoin F, Ottensmann S, Stark D, Haïle S M and Snyder G J 2005 *Adv. Funct. Mater.* **15** 1860
[6] Zhang S, Yan Z, Li Y, Chen Z and Zeng H 2015 *Angew. Chem.* **127** 3155
[7] Liu H, *et al.* 2014 *ACS Nano* **8** 4033
[8] Jaiganesh G, Britto T M A, Eithiraj R and Kalpana G 2008 *J. Phys.: Condens. Matter* **20** 085220
[9] Kalarasse F and Bennecer B 2006 *J. Phys. Chem. Solids* **67** 846
[10] He H, Tyson C and Bobev S 2011 *Inorg. Chem.* **50** 8375
[11] Prots Y, Aydemir U, Öztürk S S and Somer M 2007 *Zeitschrift für Kristallographie-New Crystal Structures* **222** 163
[12] Grotz C, Baumgartner M, Freitag K M, Baumer F and Nilges T 2016 *Inorg. Chem.* **55** 7764
[13] Gvozdetskyi V, *et al.* 2019 *Chem. Mater.* **31** 8695
[14] Ishida J, Iimura S and Hosono H 2018 *Inorg. Chem.* **57** 4997
[15] Stoyko S S, Khatun M and Mar A 2012 *Inorg. Chem.* **51** 9517
[16] Zhang T, *et al.* 2019 *Nature* **566** 475
[17] Tang F, Po H C, Vishwanath A and Wan X 2019 *Nature* **566** 486
[18] Vergniory M, *et al.* 2019 *Nature* **566** 480
[19] Wang Y Y, *et al.* 2020 *Phys. Rev. B* **102** 115122
[20] Tang F and Wan X 2019 *Frontiers of Physics* **14** 43603
[21] Toby B H 2001 *J. Appl. Crystallogr.* **34** 210
[22] Giannozzi P, *et al.* 2009 *J. Phys.: Condens. Matter* **21** 395502
[23] Giannozzi P, *et al.* 2017 *J. Phys.: Condens. Matter* **29** 465901
[24] Perdew J P, *et al.* 2008 *Phys. Rev. Lett.* **100** 136406
[25] Wolgast S, *et al.* 2013 *Phys. Rev. B* **88** 180405
[26] Ren Z, Taskin A, Sasaki S, Segawa K and Ando Y 2010 *Phys. Rev. B* **82** 241306
[27] Qu D X, Hor Y S, Xiong J, Cava R J and Ong N P 2010 *Science* **329** 821
[28] Trang C X, *et al.* 2016 *Phys. Rev. B* **93** 165123
[29] Huang X, *et al.* 2015 *Phys. Rev. X* **5** 031023
[30] Du J, *et al.* 2016 *Science China Physics, Mechanics and Astronomy* **59** 657406
[31] Li Y, *et al.* 2016 *Phys. Rev. B* **94** 121115
[32] Li H, *et al.* 2016 *Nat. Commun.* **7** 10301
[33] Ritchie L, *et al.* 2003 *Phys. Rev. B* **68** 104430
[34] Chiba H, Kikuchi M, Kusaba K, Muraoka Y and Syono Y 1996 *Solid State Commun.* **99** 499
[35] Von Molnar S and Methfessel S 1967 *J. Appl. Phys.* **38** 959
[36] Hu J, Rosenbaum T and Betts J 2005 *Phys. Rev. Lett.* **95** 186603
[37] Kawaji S 1986 *Surf. Sci.* **170** 682
[38] Lu H Z and Shen S Q 2014 *Spintronics VII* 9167: 263-273
[39] Wang Y and Santiago-Avilés J J 2003 *J. Appl. Phys.* **94** 1721
[40] Lu H Z and Shen S Q 2014 *Phys. Rev. Lett.* **112** 146601
[41] Dai X, Du Z Z and Lu H Z 2017 *Phys. Rev. Lett.* **119** 166601
[42] Breunig O, *et al.* 2017 *Nat. Commun.* **8** 15545
[43] Syers P and Paglione J 2017 *Phys. Rev. B* **95** 045123
[44] He J, *et al.* 2017 *Phys. Rev. B* **95** 195165
[45] Luo Y, *et al.* 2015 *Appl. Phys. Lett.* **107** 182411
[46] Zhao L, *et al.* 2017 *Phys. Rev. B* **95** 115119
[47] Witting I T, *et al.* 2019 *Adv. Electron. Mater.* **5** 1800904
[48] Mao J, *et al.* 2019 *Science* **365** 495